OPEN ACCESS
JOURNAL OF ADVANCED DIELECTRICS
Vol. 13, No. 6 (2023) 2345004 (9 pages)
© The Author(s)
DOI: 10.1142/S2010135X23450042

Enhanced optoelectronic characteristics of MoS_2-based photodetectors through hybridization with $CdS_{0.42}Se_{0.58}$ nanobelt*

Aimin Liu[†], Jiyu Zhao[†], Qiuhong Tan[†,‡,§,¶], Peizhi Yang[‡], Yingkai Liu[†,‡,§] and Qianjin Wang[†,‡,§,‖]

[†]*College of Physics and Electronic Information Yunnan Normal University, Yunnan Kunming 650500, P. R. China*

[‡]*Yunnan Provincial Key Laboratory for Photoelectric Information Technology Yunnan Normal University, Yunnan Kunming 650500, P. R. China*

[§]*Key Laboratory of Advanced Technique & Preparation for Renewable Energy Materials Ministry of Education Yunnan Normal University Yunnan Kunming 650500, P. R. China*

[¶]tanqiuhong1@126.com

[‖]qjwang@xtu.edu.cn

Received 22 August 2023; Revised 30 September 2023; Accepted 8 October 2023; Published 31 October 2023

Monolayer molybdenum disulfide (MoS_2) has weak light absorption due to its atomically-thin thickness, thus hindering the development of MoS_2-based optoelectronic devices. CdS_xSe_{1-x} has excellent photoelectric performance in the visible light range, and its nanostructure shows great potential in new nanoscale electronic and optoelectronic devices. In this work, a composite photodetector device with the combination of monolayer MoS_2 nanosheets and $CdS_{0.42}Se_{0.58}$ nanobelts has been successfully prepared, which can not only maintain the inherent excellent properties of the two blocks, but also play a synergistic role between them, thus improving the photoelectric performance of the device. The monolayer MoS_2 nanosheet /$CdS_{0.42}Se_{0.58}$ nanobelt photodetector has a wide spectral response range (400–800 nm), high responsivity (527.22 A/W) and large external quantum efficiency (EQE) (1.06×10^5%). Compared with the isolated monolayer MoS_2 nanosheet, both the responsivity and EQE of the hybrid photodetector are increased by 117.4 times under 620 nm illumination. This study provides a way to prepare hybrid photodetectors with wide spectral response and high responsivity.

Keywords: Monolayer MoS_2; $CdS_{0.42}Se_{0.58}$ nanobelt; photodetectors.

1. Introduction

The photodetector device can utilize the photoelectric effect to convert light information into electrical signals, achieving the function of the information transmission.[1] It has wide applications in both civilian and military fields such as optical communication, biomedical imaging, automation control and military early warning.[2–6] Transition metal dichalcogenides are typical two-dimensional semiconductors with an X–M–X structure (M = Mo, W, Nb, Ta, Ti, Re; X = S, Se, or Te), which possess advantages such as tunable band gaps, high carrier mobility and luminescent properties and thus have been extensively studied in photoelectronic devices.[7–9] Among them, MoS_2 as a representative transition metal dichalcogenide has been widely explored in field-effect transistors, photodetectors and solar cells.[10–16] Bulk MoS_2 has an indirect band gap with a value of 1.3 eV. When transitioning from bulk to monolayer, the band gap changes from indirect to direct, resulting in a band gap value of 1.8 eV for monolayer MoS_2.[17] With the change of band gap, MoS_2 also exhibits various unique properties. The carrier mobility of MoS_2 decreases with the decrease of the number of layers at room temperature, and when the number of layers gradually decreases to a monolayer, the relaxation speed of electrons between the conduction and valence bands slows down, leading to increased intensity, reduced full width at half maximum and enhanced fluorescence efficiency of the photoluminescence (PL) peak.[18] Currently, MoS_2 photodetectors have exhibited promising device performance. However, due to limited light absorption capacity of monolayer MoS_2 and constraints imposed by significant excitonic effects on the separation of photo-generated carriers, photodetectors based solely on MoS_2 still face many shortcomings. These include issues like prolonged device response times, relatively low device currents and responsivity, indicating further work is needed to improve the device performance. Lopez-Sanchez *et al.*[12] reported an ultra-sensitive monolayer MoS_2 photodetector with a high responsivity of 880 A/W. However, this device has a very long response/recovery time, exceeding 100 s. Considering the challenges faced by monolayer MoS_2

*This paper was originally submitted to the Special Issue on Ferroelectric Nanoelectronic Devices for Next-Generation Information Technology organized by Zheng Wen, Shuoguo Yuan, Zhen Fan and Yunya Liu.

This is an Open Access article published by World Scientific Publishing Company. It is distributed under the terms of the Creative Commons Attribution 4.0 (CC BY) License which permits use, distribution and reproduction in any medium, provided the original work is properly cited.

photodetectors, the best solution is to construct hybrid composite structures.[19,20]

Ternary alloy chalcogenide compounds, such as CdS_xSe_{1-x} nanostructures, have garnered significant global attention due to their excellent tunable optical properties based on quantum confinement effects and optical nonlinear phenomena.[21–23] Nanostructures based on CdS_xSe_{1-x}, such as zero-dimensional quantum dots or nanocrystals, one-dimensional nanowires and nanobelts, as well as two-dimensional nanosheets, exhibit potential applications in fluorescence labeling,[24,25] *in vivo* imaging,[26] waveguides,[27] solar cells[28] and photodetectors.[29–31] In recent years, various structures of CdS_xSe_{1-x} ternary alloy-based photodetectors have been reported, and exhibited exceptional photoelectric performance. In 2015, Guo *et al.*[22] designed a broad spectral response photodetector based on CdS_xSe_{1-x} nanowires with gradient bandgap, achieving light response from ultraviolet to 700 nm. It exhibited good photocurrent and photoconductivity at room and low temperatures, with a dark-to-light current ratio of up to 10^6. In 2018, Li *et al.*[32] fabricated a single $CdS_{0.76}Se_{0.24}$ nanobelt photodetector via thermal evaporation, offering a new strategy for designing wavelength-controllable photodetectors. It displayed excellent photoelectric performance with a response of 10.4 A/W and an external quantum efficiency (EQE) of 1.90×10^3% under 1 V bias and 674 nm light illumination, and a response time of 1.62/4.70 ms. To enhance the spectral response range of CdSSe-based photodetectors, Moger *et al.*[33] deposited *n*-CdS_xSe_{1-x} thin films on *p*-Si using thermal co-evaporation in 2021, subsequently fabricating *p-n* junction photodiodes and investigating the effects of composition on the structure, optical and electrical properties. They found that the photodiode displayed a high responsivity of 0.11 A/W at 635 nm light when $x = 0.2$. Until now, there have been few reports on the hybrid photodetectors based on single-layer MoS_2 and CdS_xSe_{1-x} nanobelts.

In this study, we have fabricated a hybrid photodetector by dry transfer $CdS_{0.42}Se_{0.58}$ nanobelt onto a monolayer MoS_2 nanosheet. The hybrid device shows a significant enhancement in spectral response within the visible light range (400–800 nm). Compared to the monolayer MoS_2 nanosheet device, the hybrid device exhibits a remarkable increase in responsivity, EQE under 620 nm illumination and 1 V bias, with both improvements of 117.4 times. The enhanced photoelectric performance of the hybrid device is explained through the appropriate band alignment of MoS_2 and $CdS_{0.42}Se_{0.58}$, providing insight into the underlying microscopic mechanisms. This work offers a potential pathway for the construction of high-performance visible light photodetectors.

2. Experimental

2.1. *Device fabrication*

The preparation of monolayer MoS_2 nanosheets utilized MoO_3 (99.999% purity) as the molybdenum source and solid-state sulfur (99.999% purity) as the sulfur source, with argon gas serving as the work gas. A double-temperature-zone tube furnace with an 80 mm diameter was used. The MoO_3 was heated to 650°C, while sulfur was heated to 180°C, under a growth pressure of 4000 Pa. The growth process lasted for 10 min. This method yielded high-quality monolayer MoS_2 on the substrate. Subsequently, the very thin Cr/Au electrodes were deposited on it.

The $CdS_{0.42}Se_{0.58}$ nanobelts were obtained from previous research work.[34] The fabricated $CdS_{0.42}Se_{0.58}$ nanobelts were visually inspected under a microscope, the regions with smooth surfaces as well as thin growth thickness were chosen and then was scraped into small test tubes with tweezers. Then, anhydrous ethanol was added and shaken from side to side. Next, the $CdS_{0.42}Se_{0.58}$ solution was dropped onto a 1.5 cm × 1.5 cm silicon wafer. Finally, the $CdS_{0.42}Se_{0.58}$ nanobelts were transferred onto the monolayer MoS_2 substrate with pre-deposited electrodes with the help of PDMS film.

2.2. *Performance characterization*

Optical properties were measured using Raman spectroscopy (SR-500i-B2) and PL spectroscopy (IK3301). The photoelectric performance of the devices was tested using a semiconductor measurement system (Keithley 4200SCS) and a monochromator (Newport CS260). Device photocurrent was measured by changing the incident light vertically shining on the device. The *I-V* and *I-t* curves were measured using a double-probe technique.

3. Results and Discussion

Figure 1(a) shows the optical image of the prepared MoS_2 nanosheets, in which triangularly distributed MoS_2 nanosheets are observed on a silicon dioxide substrate, exhibiting a smooth surface, with a maximum side length of approximately 30 μm. Figure 1(b) presents the Raman spectroscopy of the MoS_2 nanosheets obtained under 532 nm laser excitation. The spectroscopic analysis serves as strong evidence for determining the material's monolayer nature. Two distinct characteristic peaks can be observed, i.e., A_{1g} and E^1_{2g} modes, whichcorrespond to out-of-plane vibrational modes of sulfur atoms and in-plane optical modes, respectively. The difference between these two peaks is related to the number of layers in the MoS_2 structure.[35] In Fig. 1(b), the observed peak separation is 18.4, highly consistent with previous literature reports,[36,37] confirming the monolayer nature of the MoS_2 nanosheets. Figure 1(c) displays the PL spectrum of the MoS_2 nanosheets excited by a 532 nm light source. A single emission peak is observed at 676 nm, corresponding to an optical bandgap of 1.83 eV, in good agreement with other experimental results.[37] This further indicated that the prepared MoS_2 nanosheets are indeed a monolayer structure.

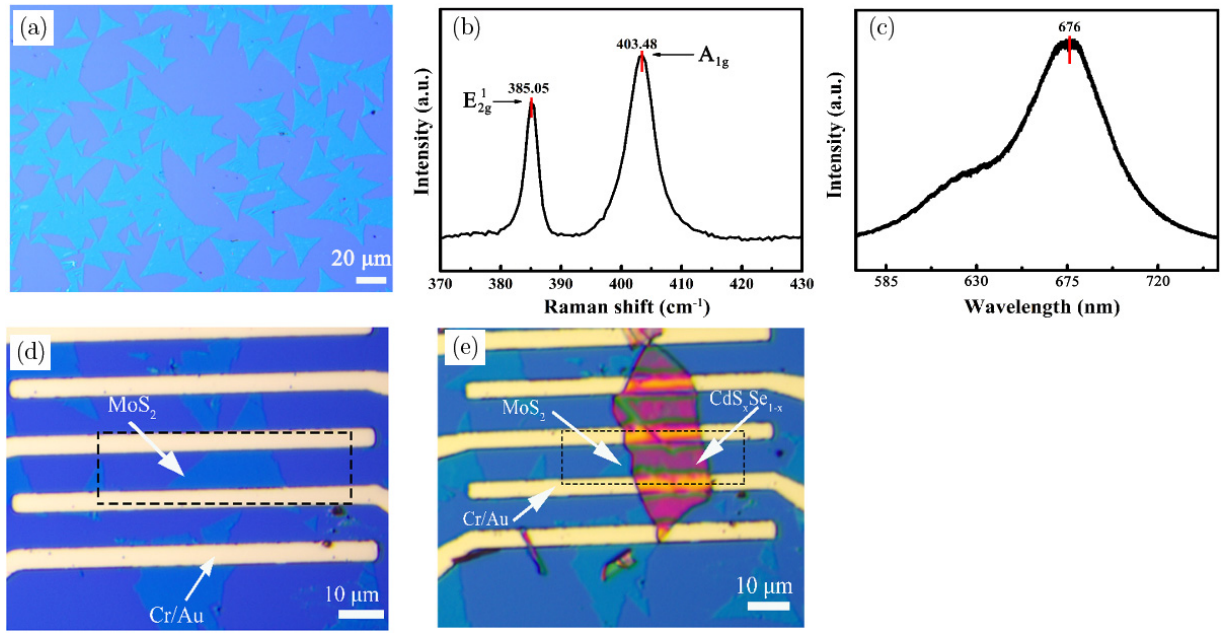

Fig. 1. (a) The optical microscope image, (b) Raman spectrum and (c) PL spectrum of the prepared MoS_2 nanosheets, (d) Optical image of the monolayer MoS_2 nanosheet device and (e) Optical image of the monolayer MoS_2 nanosheet/$CdS_{0.42}Se_{0.58}$ nanobelt device.

Figure 1(d) depicts the optical image of the prepared MoS_2 nanosheet device. The yellow regions represent Cr/Au electrodes with a spacing of 10 μm, the deep blue portion corresponds to the silicon dioxide substrate, and the teal-blue triangular morphology represents the MoS_2 nanosheets. The rectangular dashed box outlines the designated measurement region for the device, with an area of 2.0×10^{-6} cm^2. Figure 1(e) illustrates the composite device consisting of $CdS_{0.42}Se_{0.58}$ nanobelt transferred onto monolayer MoS_2 nanosheet using a transfer platform. The pink regions with belt-like morphology represent $CdS_{0.42}Se_{0.58}$ nanobelt and the composite device has an area of 2.6×10^{-6} cm^2.

Figures 2(a) and 2(b) show the *I*-*V* curve of a monolayer MoS_2 nanosheet device under 620 nm light illumination with a light power density of 0.110 mW/cm^2. At a bias voltage of 1 V, the photocurrent is measured to be 3.48×10^{-10} A, while the dark current is 2.82×10^{-12} A, resulting in an on/off ratio of 1.24×10^2. This on/off ratio is quite consistent with previously reported monolayer MoS_2 nanosheet photodetectors.[38] It is evident that due to the thickness limitation of the monolayer MoS_2 nanosheet, the photocurrent of the device is extremely small.

We next investigated the variation of photocurrent with light power density for the device under 620 nm illumination, as shown in Figs. 2(c) and 2(d). It is observed that the photocurrent continuously increases with increasing light power density under bias voltages of −1–1 V. The maximum photocurrent is achieved at a light power density of 0.110 mW/cm^2, while the minimum is observed at 0.014 mW/cm^2. This behavior indicates that the efficiency of photogenerated charge carriers is directly proportional to the absorption efficiency of photons. Figure 2(e) presents the relationship between the photocurrent of MoS_2 nanosheet photodetector and light power density at different levels. The fitted exponent value θ of the formula $I_p = AP^\theta$ is found to be 0.539. This suggests that the monolayer MoS_2 nanosheet device undergoes complex processes involving the generation, separation, capture and recombination of electron-hole pairs.[38] To further explore the device's photoelectric performance, we conducted calculations and analysis for key parameters such as responsivity (R) and EQE. The calculation formulas are as follows:

$$R = \frac{I_p - I_d}{P \times A}, \tag{1}$$

$$\mathrm{EQE} = \frac{1240}{\lambda} \times R, \tag{2}$$

where I_p and I_d represents the photocurrent and dark current, P stands for light power density, A denotes the device area and λ (nm) is the wavelength of the incident light. Figure 2(f) illustrates the relationship between spectral response and EQE of the monolayer MoS_2 nanosheet photodetector under 620 nm illumination as a function of light power density. It is observed that with increasing light power density, the spectral response and EQE of the device gradually decrease, indicating the presence of non-negligible recombination losses in the system. Additionally, it can be observed that at a light power density of 0.014 mW/cm^2 and a bias voltage of 1 V, the device achieves its maximum responsivity (R) and EQE, reaching maximum values of 4.49 A/W and 899.64%, respectively. Response speed is one of the crucial parameters for describing the performance of a photodetector.

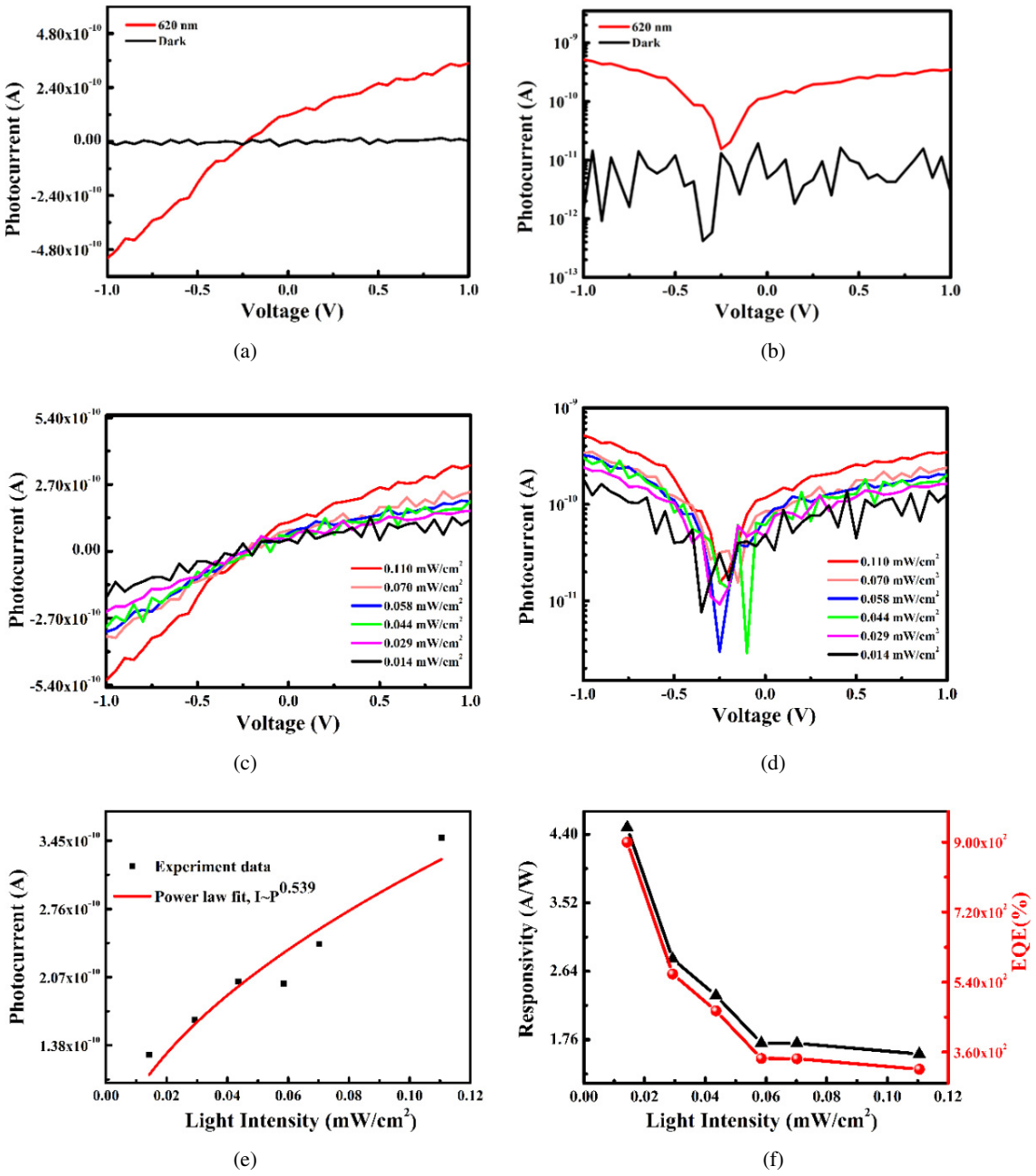

Fig. 2. The photoelectric performance of the monolayer MoS_2 nanosheet photodetector under 620 nm. (a) *I-V* curve and (b) *I-V* logarithmic curve at a light power density of 0.110 mW/cm^2, (c) *I-V* curves of the device at various light power densities and (d) corresponding *I-V* logarithmic curves, (e) The relationship between the photocurrent and light power density and (f) The spectral response and EQE as a function of light power density.

The rise/fall time is defined as the time required for the photocurrent to transition from 10%/90% to 90%/10% of the saturation value. Figure 3(a) presents the photo-switching behavior of the monolayer MoS_2 nanosheet photodetector, indicating good switching stability of the device. From Fig. 3(b), it can be inferred that the rise/fall time of the device is approximately 43.3/77.6 ms. Figure 3(c) presents the spectral response graphs of the monolayer MoS_2 nanosheet, $CdS_{0.42}Se_{0.58}$ nanobelt and monolayer MoS_2 nanosheet/$CdS_{0.42}Se_{0.58}$ nanobelt composite devices. It can be observed that the spectral response of the device significantly enhances in the wavelength range of 400–800 nm after the monolayer MoS_2 nanosheet combined with the $CdS_{0.42}Se_{0.58}$ nanobelt. Particularly, the device exhibits notably higher response values under 560 nm and 620 nm light irradiation.

Figures 4(a) and 4(b) show the *I-V* curves of monolayer MoS_2 nanosheet/$CdS_{0.42}Se_{0.58}$ nanobelt photodetector under 620 nm light illumination at bias voltages of −1–1 V and a

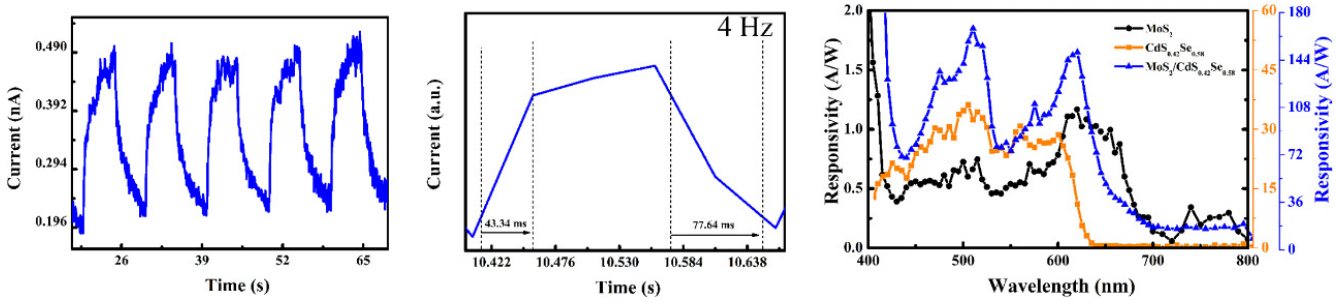

(a) (b) (c)

Fig. 3. (a) Periodic *I-t* curve and (b) individual *I-t* curve of the MoS_2 nanosheet photodetector under 620 nm light with a power density of 0.110 mW/cm^2; (c) Spectral response of the monolayer MoS_2 nanosheet, $CdS_{0.42}Se_{0.58}$ nanobelt and monolayer MoS_2 nanosheet/$CdS_{0.42}Se_{0.58}$ nanobelt composite devices.

light power density of 0.110 mW/cm^2. At a bias voltage of 1 V, the photocurrent and dark current are measured to be 6.26×10^{-8} A and 2.99×10^{-10} A, respectively, resulting in an on/off ratio of 2.09×10^2. Compared to the monolayer MoS_2 nanosheet device, both the photocurrent and dark current of the composite device have increased by around two orders of magnitude, leading to little change in the device's on/off ratio. From Figs. 4(c) and 4(d), it can be observed that the photocurrent of the device increases with the increment of light power density under 620 nm illumination. The *I-V* curve

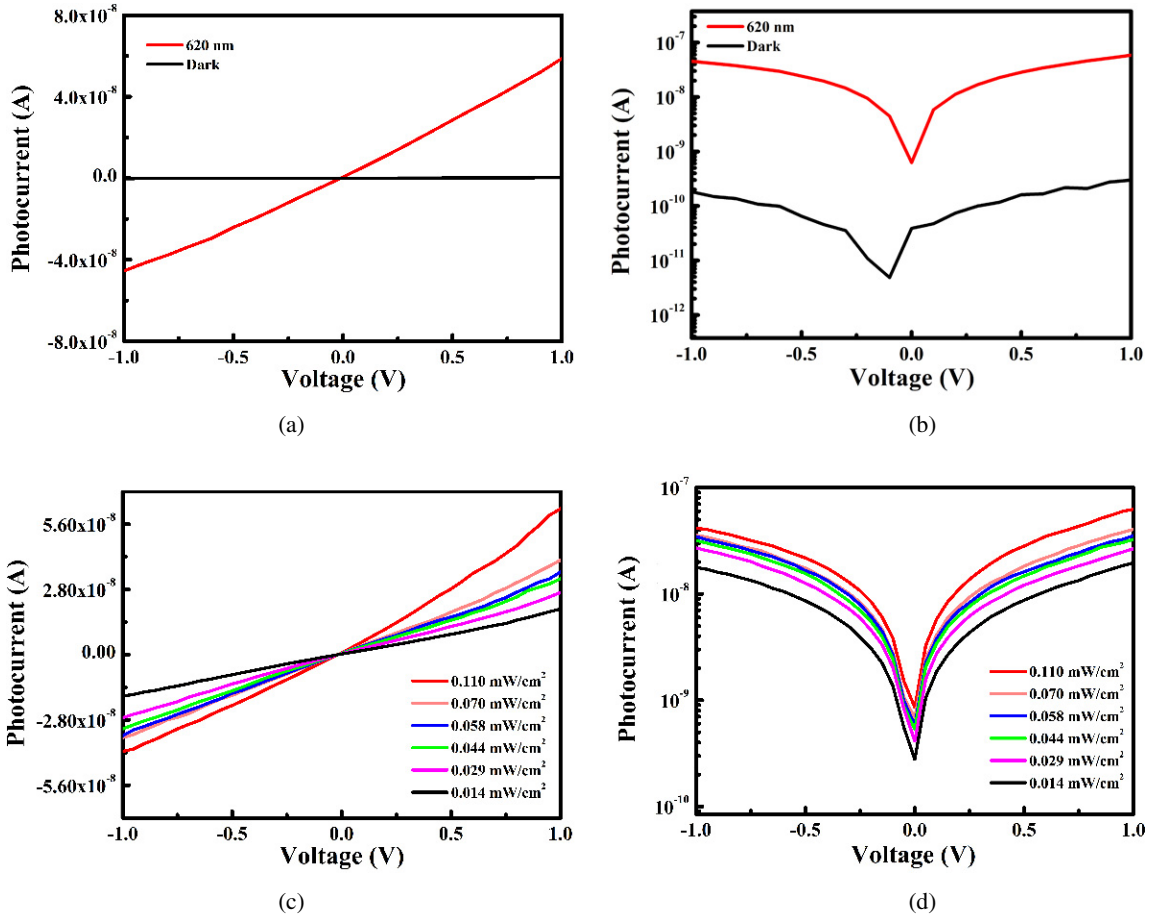

(a) (b) (c) (d)

Fig. 4. The photoelectric performance of the monolayer MoS_2 nanosheet/$CdS_{0.42}Se_{0.58}$ nanobelt photodetector under 620 nm. (a) *I-V* curve and (b) *I-V* logarithmic curve at a light power density of 0.110 mW/cm^2; (c) *I-V* curves of the device at various light power densities and (d) corresponding *I-V* logarithmic curves; (e) The relationship between the photocurrent and light power density and (f) The spectral response and EQE as a function of light power density.

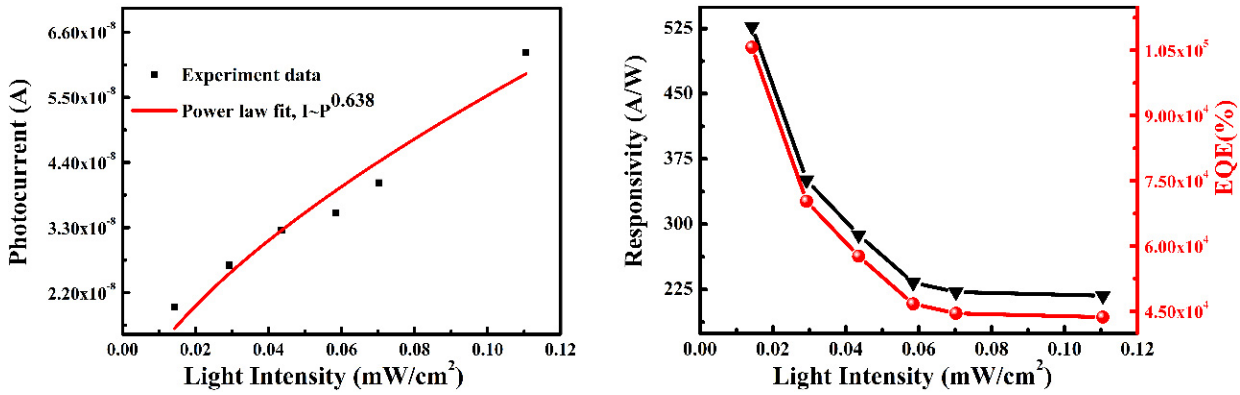

(e) (f)

Fig. 4. (*Continued*)

exhibits linearity and the photocurrent is almost symmetric at −1 V and 1 V bias, indicating good Ohmic contact between the nanobelt and the electrodes. By fitting the formula $I_p = AP^{\theta}$, the fitted exponent θ is determined to be 0.638 (see Fig. 4(e)). This suggests the presence of trap states in the monolayer MoS_2 nanosheet/$CdS_{0.42}Se_{0.58}$ nanobelt hybrid device, leading to significant recombination losses. Figure 4(f) depicts the relationship between R and EQE of the monolayer MoS_2 nanosheet/$CdS_{0.42}Se_{0.58}$ nanobelt device with changing light power density. At a light power density of 0.014 mW/cm^2, the device's R, and EQE are measured to be 527.22 A/W and 1.06 × 105%, respectively. In comparison to the monolayer MoS_2 nanosheet device under the same bias and light power density, the composite device exhibits significant improvements in its R and EQE value, which both have a 117.4-fold improvement. These results highlight a significant enhancement in the photoelectric performance of the monolayer MoS_2 nanosheet/$CdS_{0.42}Se_{0.58}$ nanobelt composite device.

Figures 5(a) and 5(b) show the variation of photocurrent with time for the monolayer MoS_2 nanosheet/$CdS_{0.42}Se_{0.58}$ nanobelt photodetector. It can be observed that the device maintains good stability in terms of both photocurrent and dark current. The rise/fall time of the device is approximately 38.9/82.7 ms. Compared to the rise/fall time of around 43.3/77.6 ms for the monolayer MoS_2 nanosheet photodetector, the response time of the device has no significant change.

The performance of the as-fabricated monolayer MoS_2 nanosheet/$CdS_{0.42}Se_{0.58}$ nanobelt photodetector was compared with the reported MoS_2-based photodetectors, and the key parameters were summarized in Table 1. It is evident that the monolayer MoS_2 nanosheet/$CdS_{0.42}Se_{0.58}$ nanobelt photodetector exhibits certain advantages in terms of EQE and R, compared to other MoS_2-based photodetectors.

To elucidate the mechanism behind the enhanced performance of the monolayer MoS_2 nanosheet/$CdS_{0.42}Se_{0.58}$ nanobelt photodetector, we analyzed it from the perspective of the energy band alignment of the two materials. Before the MoS_2 nanosheet and $CdS_{0.42}Se_{0.58}$ nanobelt contact, the electrons are excited to the conduction band while leaving holes in the valence band when the incident light energy is greater than the band gap of the material. Under bias,

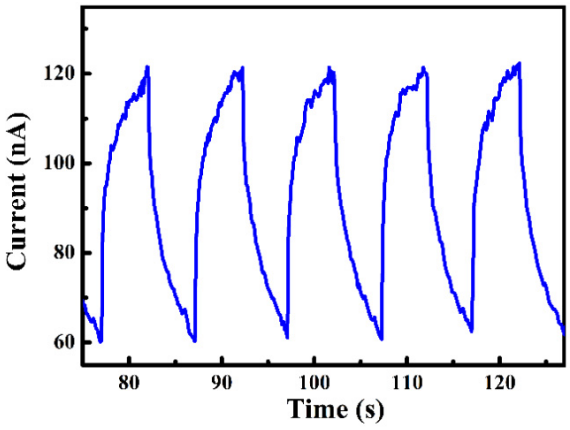

(a)

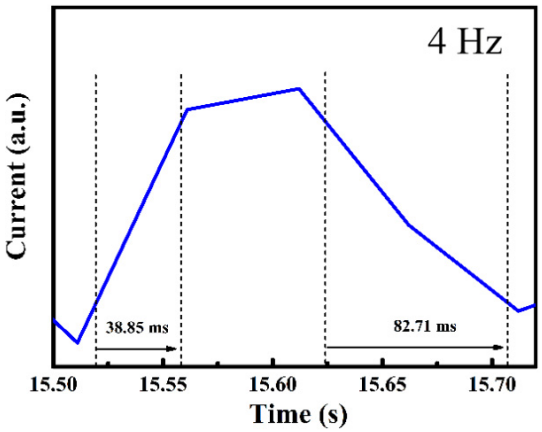

(b)

Fig. 5. (a) Periodic *I-t* curve and (b) individual *I-t* curve of the monolayer MoS_2 nanosheet/$CdS_{0.42}Se_{0.58}$ nanobelt photodetector.

Table 1. Comparison of key parameters of MoS_2-based photodetectors.

Device structure	Bias voltage	λ (nm)	EQE (%)	R (A/W)	Rise/decay time	Ref.
1 L MoS_2	8 V	561	—	880	4/9 s	12
n-MoS_2/p-Si	10 V	441	—	1.04×10^{-2}	1.56/1.18 ms	39
1 L MoS_2/$CsPbBr_3$ NCs	10 V	405	—	24.34	5.5/24 μs	40
n-MoS_2/n-ZnO	5 V	532	80.9	0.35	1.3/2.2 s	41
1 L MoS_2	1 V	620	8.99×10^2	4.49	43.3/77.6 ms	This
1 L MoS_2/$CdS_{0.42}Se_{0.58}$ NB	1 V	620	1.06×10^5	527.22	38.9/82.7 ms	Work

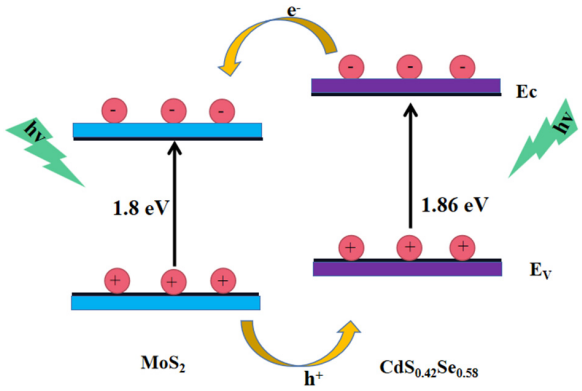

Fig. 6. The electron transfer process in the monolayer MoS_2 nanosheet/$CdS_{0.42}Se_{0.58}$ nanobelt composite photodetector under photoexcitation.

electrons and holes flow in opposite directions, and generate photocurrent. However, after the combination of MoS_2 nanosheet and $CdS_{0.42}Se_{0.58}$ nanobelt, they form a type-II band alignment structure based on the previous literature reported,[42,43] which facilitates the effective separation of photo-generated charge carriers. Under illumination, the photoexcited electrons transfer from the conduction band of $CdS_{0.42}Se_{0.58}$ to the conduction band of MoS_2, and conversely, holes transfer from the valence band of MoS_2 to the valence band of $CdS_{0.42}Se_{0.58}$, is illustrated in Fig. 6. This achieves the separation of electrons and holes, leading to an increase in photocurrent. Consequently, the photoelectric performance of the monolayer MoS_2 nanosheet/$CdS_{0.42}Se_{0.58}$ nanobelt photodetector is enhanced compared to the monolayer MoS_2 nanosheet device.

4. Conclusions

In summary, monolayer MoS_2 nanosheets and $CdS_{0.42}Se_{0.58}$ nanobelts were first prepared using the chemical vapor deposition method. Subsequently, a composite device comprising monolayer MoS_2 nanosheet/$CdS_{0.42}Se_{0.58}$ nanobelt was fabricated through a dry transfer process. This composite device exhibited enhanced spectral response within the range of 400–800 nm. A comparison with the monolayer MoS_2 nanosheet device and the composite device showed significant improvements in R and EQE, which increased by 117.4 times. The enhanced photoelectric performance of the composite device is attributed to the type-II band alignment formed between MoS_2 and $CdS_{0.42}Se_{0.58}$. Under illumination, photo-generated electrons transferred from the conduction band of $CdS_{0.42}Se_{0.58}$ to that of MoS_2, and conversely, holes transferred from the valence band of MoS_2 to that of $CdS_{0.42}Se_{0.58}$. This facilitated the separation of electrons and holes, resulting in increased photocurrent. As a result, the performance of the monolayer MoS_2 nanosheet/$CdS_{0.42}Se_{0.58}$ nanobelt photodetector was enhanced compared to using a single material alone, providing a promising strategy for constructing high-performance photodetectors.

Acknowledgments

This work was supported by the National Natural Science Foundation of China (Nos. 11864046 and 11764046), the Basic Research Program of Yunnan Province (Nos. 202001AT070064 and 202101AT070124), Spring City Plan: the High-level Talent Promotion and Training Project of Kunming (2022SCP005).

ORCID

Qiuhong Tan https://orcid.org/0000-0003-0181-341X
Peizhi Yang https://orcid.org/0000-0002-7769-4499
Yingkai Liu https://orcid.org/0000-0003-0041-1793
Qianjin Wang https://orcid.org/0000-0003-1474-0918

References

[1] Y. L. Tang and J. Chen, High responsivity of Gr/n-Si schottky junction near-infrared photodetector, *Superlattices Microstruct.* **8**, 150 (2021).
[2] R. D. Jansen-van Vuuren, A. Armin, A. K. Pandey, P. L. Burn and P. Meredith, Organic photodiodes: The future of full color detection and image sensing, *Adv. Mater.* **28**, 4766 (2016).
[3] J. P. Zeng, C. F. Meng, X. M. Li, Y. Wu, S. T. Liu, H. Zhou, H. Wang and H. B. Zeng, Interfacial-tunneling-effect-enhanced $CsPbBr_3$ photodetectors featuring high detectivity and stability, *Adv. Funct. Mater.* **9**, 29 (2019).
[4] M. Yang, Q. Han, X. C. Liu, J. Y. Han, Y. F. Zhao, L. He, J. Gou, Z. M. Wu, X. R. Wang and J. Wang, Ultrahigh stability 3D TI Bi_2Se_3/MoO_3 thin film heterojunction infrared photodetector at optical communication waveband, *Adv. Funct. Mater.* **8**, 30 (2020).

[5]X. Huang, Y. L. Guo and Y. Q. Liu, Perovskite photodetectors and their application in artificial photonic synapses, *Chem. Commun.* **57**, 11429 (2021).
[6]C. Wu, F. M. Wu and D. Y. Guo, Review of self-powered solar-blind photodetectors based on Ga_2O_3, *Mater. Today Phys.* **28**, 100883 (2022).
[7]X. D. Duan, C. Wang, A. L. Pan, R. Q. Yu and X. F. Duan, Two-dimensional transition metal dichalcogenides as atomically thin semiconductors: Opportunities and challenges, *Chem. Soc. Rev.* **44**, 8859 (2015).
[8]X. Tong, E. Ashalley, F. Lin, H. D. Li and Z. M. M. Wang, Advances in MoS_2-based field effect transistors (FETs), *Nano-Micro Lett.* **7**, 203 (2015).
[9]K. P. Dhakal, D. L. Duong, J. Lee, H. Nam, M. Kim, M. Kan, Y. H. Lee and J. Kim, Confocal absorption spectral imaging of MoS_2: Optical transitions depending on the atomic thickness of intrinsic and chemically doped MoS_2, *Nanoscale* **6**, 13028 (2014).
[10]B. Radisavljevic, A. Radenovic, J. Brivio, V. Giacometti and A. Kis, Single-layer MoS_2 transistors, *Nat. Nanotechnol.* **6**, 147 (2011).
[11]F. Y. Liao, Y. C. Sheng, Z. X. Guo, H. W. Tang, Y. Wang, L. Y. Zong, X. Y. Chen, A. Riaud, J. H. Zhu, Y. F. Xie, L. Chen, H. Zhu, Q. Q. Sun, P. Zhou, X. W. Jiang, J. Wan, W. Z. Bao and D. W. Zhang, MoS_2 dual-gate transistors with electrostatically doped contacts, *Nano Res.* **12**, 2515 (2019).
[12]O. Lopez-Sanchez, D. Lembke, M. Kayci, A. Radenovic and A. Kis, Ultrasensitive photodetectors based on monolayer MoS_2, *Nat. Nanotechnol.* **8**, 497 (2013).
[13]T. Noh, H. S. Shin, C. Seo, J. Y. Kim, J. Youn, J. Kim, K. S. Lee and J. Joo, Significant enhancement of photoresponsive characteristics and mobility of MoS_2-based transistors through hybridization with perovskite $CsPbBr_3$ quantum dots, *Nano Res.* **12**, 405 (2019).
[14]M. L. Tsai, S. H. Su, J. K. Chang, D. S. Tsai, C. H. Chen, C. I. Wu, L. J. Li, L. J. Chen and J. H. He, Monolayer MoS_2 heterojunction solar cells, *ACS Nano* **8**, 8317 (2014).
[15]W. Zhang and F. Qiu, Lattice defect engineering enables performance-enhanced MoS_2 photodetector through a paraelectric $BaTiO_3$ dielectric, *ACS Nano* **15**, 13370 (2021).
[16]T. Hu and F. Qiu, Photodetectors based on two-dimensional MoS_2 and its assembled heterostructures, *Chip* **1**, 100017 (2022).
[17]R. Ganatra and Q. Zhang, Few-layer MoS_2: A promising layered semiconductor, *ACS Nano* **8**, 4074 (2014).
[18]K. F. Mak, C. Lee, J. Hone, J. Shan and T. F. Heinz, Atomically thin MoS_2: A new direct-gap semiconductor, *Phys. Rev. Lett.* **4**, 105 (2010).
[19]W. J. Zhang, C. P. Chuu, J. K. Huang, C. H. Chen, M. L. Tsai, Y. H. Chang, C. T. Liang, Y. Z. Chen, Y. L. Chueh, J. H. He, M. Y. Chou and L. J. Li, Ultrahigh-Gain photodetectors based on atomically thin graphene-MoS_2 heterostructures, *Sci. Rep.* **8**, 4 (2014).
[20]X. P. Hong, J. Kim, S. F. Shi, Y. Zhang, C. H. Jin, Y. H. Sun, S. Tongay, J. Q. Wu, Y. F. Zhang and F. Wang, Ultrafast charge transfer in atomically thin MoS_2/WS_2 heterostructures, *Nat. Nanotechnol.* **9**, 682 (2014).
[21]C. J. Ding, T. Q. Lu, N. Wazir, W. F. Ma, S. Guo, Y. Xin, A. Li, R. B. Liu and B. S. Zou, New type of thermoelectric CdSSe nanowire chip, *ACS Appl. Mater. Interfaces* **13**, 30959 (2021).
[22]S. Guo, Z. S. Li, G. L. Song, B. S. Zou, X. X. Wang and R. B. Liu, Large-area photodetector with high-sensitivity and broadband spectral response based on composition-graded CdSSe nanowire-chip, *J. Alloys Compd.* **649**, 793 (2015).
[23]A. L. Pan, H. Yang, R. C. Yu and B. S. Zou, Fabrication and photoluminescence of high-quality ternary CdSSe nanowires and nanoribbons, *Nanotechnology* **17**, 1083 (2006).
[24]P. Alivisatos, The use of nanocrystals in biological detection, *Nat. Biotechnol.* **22**, 47 (2004).
[25]E. Petryayeva and W. R. Algar, Multiplexed homogeneous assays of proteolytic activity using a smartphone and quantum dots, *Anal. Chem.* **86**, 3195 (2014).
[26]J. P. Zimmer, S. W. Kim, S. Ohnishi, E. Tanaka, J. V. Frangioni and M. G. Bawendi, Size series of small indium arsenide-zinc selenide core-shell nanocrystals and their application to *in vivo* imaging, *J. Am. Chem. Soc.* **128**, 2526 (2006).
[27]A. L. Pan, R. B. Liu, F. F. Wang, S. S. Xie, B. S. Zou, M. Zacharias and Z. L. Wang, High-quality alloyed CdS_xSe_{1-x} whiskers as waveguides with tunable stimulated emission, *J. Phys. Chem. B* **110**, 22313 (2006).
[28]X. H. Song, M. Q. Wang, J. P. Deng, Z. Yang, C. M. Ran, X. Y. Zhang and X. Yao, One-step preparation and assembly of aqueous colloidal CdS_xSe_{1-x} nanocrystals within mesoporous TiO_2 films for quantum dot-sensitized solar cells, *ACS Appl. Mater. Interfaces* **5**, 5139 (2013).
[29]T. Takahashi, P. Nichols, K. Takei, A. C. Ford, A. Jamshidi, M. C. Wu, C. Z. Ning and A. Javey, Contact printing of compositionally graded CdS_xSe_{1-x} nanowire parallel arrays for tunable photodetectors, *Nanotechnology* **4**, 23 (2012).
[30]M. Elisa, C. Vasiliu, J. Striber, D. Radu, J. H. Trodahl and M. Dalley, Optical and structural investigations on Cd-S-Se-doped aluminophosphate glasses, *J. Optoelectron. Adv. Mater.* **8**, 811 (2006).
[31]P. O. Anikeeva, J. E. Halpert, M. G. Bawendi and V. Bulovic, Quantum dot light-emitting devices with electroluminescence tunable over the entire visible spectrum, *Nano Lett.* **9**, 2532 (2009).
[32]X. M. Li, Q. H. Tan, X. B. Feng, Q. J. Wang and Y. K. Liu, Wavelength-controlled photodetector based on single CdSSe nanobelt, *Nanoscale Res. Lett.* **8**, 13 (2018).
[33]S. N. Moger and M. G. Mahesha, Investigation on spectroscopic and electrical properties of p-Si/CdS_xSe_{1-x} ($0 <= x <= 1$) heterostructures for photodetector applications, *J. Alloys Compd.* **9**, 870 (2021).
[34]J. Y. Zhao and Q. J. Wang, High-performance photodetectors based on Au nanoislands decorated CdSSe nanobelt, *Acta Phys. Sin.* **72**, 098103 (2023).
[35]M. Buscema, G. A. Steele, H. S. J. van der Zant and A. Castellanos-Gomez, The effect of the substrate on the Raman and photoluminescence emission of single-layer MoS_2, *Nano Res.* **7**, 561 (2014).
[36]F. Bai, J. J. Qi, F. Li, Y. Y. Fang, W. P. Han, H. L. Wu and Y. Zhang, A high-performance self-powered photodetector based on monolayer MoS_2/perovskite heterostructures, *Adv. Mater. Interfaces* **9**, 5 (2018).
[37]L. Xu, L. Y. Zhao, Y. S. Wang, M. C. Zou, Q. Zhang and A. Y. Cao, Analysis of photoluminescence behavior of high-quality single-layer MoS_2, *Nano Res.* **12**, 1619 (2019).
[38]R. Singh, C. Patel, P. Kumar, M. Dubey, S. Sriram and S. Mukherjee, High detectivity and fast MoS_2 monolayer MSM photodetector, *ACS Appl. Electron. Mater.* **4**, 5739 (2022).

[39]H. Ahmad, H. Rashid and M. F. Ismail, Investigation of structural and optoelectronic properties of n-MoS_2/p-Si sandwiched heterojunction photodetector, *Optik* **198**, 163237 (2019).
[40]J. Ghosh, L. P. L. Mawlong, G. B. Manasa, A. J. Pattison, W. Theis, S. Chakraborty and P. K. Giri, Solid-state synthesis of stable and color tunable cesium lead halide perovskite nanocrystals and the mechanism of high-performance photodetection in a monolayer MoS_2/$CsPbBr_3$ vertical heterojunction, *J. Mater. Chem. C* **8**, 8917 (2020).
[41]J. Zhang, Y. T. Liu, X. L. Zhang, Z. Y. Ma, J. Li, C. Zhang, A. Shaikenova, B. Renat and B. D. Liu, High-performance ultraviolet-visible light-sensitive 2D-MoS_2/1D-ZnO heterostructure photodetectors, *ChemistrySelect* **5**, 3438 (2020).
[42]Y. D. Yuan, X. H. Zhang, H. W. Liu, T. F. Yang, W. H. Zheng, B. Y. Zheng, F. Jiang, L. H. Li, D. Li, X. L. Zhu and A. L. Pan, Growth of CdSe/MoS_2 vertical heterostructures for fast visible-wavelength photodetectors, *J. Alloys Compd.* **815**, 152309 (2020).
[43]W. Zheng, W. Feng, X. Zhang, X. S. Chen, G. B. Liu, Y. F. Qiu, T. Hasan, P. H. Tan and P. A. Hu, Anisotropic growth of nonlayered CdS on MoS_2 monolayer for functional vertical heterostructures, *Adv. Funct. Mater.* **26**, 2648 (2016).